Accepted Manuscript

Seismic explosion sources on an ice cap – technical considerations

Alexey Shulgin , Hans Thybo

PII: S1873-9652(14)00079-6

DOI: 10.1016/j.polar.2014.11.002

Reference: POLAR 232

To appear in: *Polar Science*

Received Date: 6 May 2014

Revised Date: 12 November 2014

Accepted Date: 26 November 2014

Please cite this article as: Shulgin, A., Thybo, H., Seismic explosion sources on an ice cap – technical considerations, *Polar Science* (2015), doi: 10.1016/j.polar.2014.11.002.

Seismic explosion sources on an ice cap – technical considerations

Alexey Shulgin[1] and Hans Thybo[2]

1. *Helmholtz Center for Ocean Research Kiel (GEOMAR), Kiel, Germany.*
2. *IGN, Geology section, Copenhagen University, Copenhagen, Denmark.*

Corresponding author: Alexey Shulgin

E-mail: ashulgin@geomar.de

Abstract

Controlled source seismic investigation of crustal structure below ice covers is an emerging technique. We have recently conducted an explosive refraction/wide-angle reflection seismic experiment on the ice cap in east-central Greenland. The data-quality is high for all shot points and a full crustal model can be modelled. A crucial challenge for applying the technique is to control the sources. Here, we present data that describe the efficiency of explosive sources in the ice cover. Analysis of the data shows, that the ice cap traps a significant amount of energy, which is observed as a strong ice wave. The ice cap leads to low transmission of energy into the crust such that charges need be larger than in conventional onshore experiments to obtain reliable seismic signals. The strong reflection coefficient at the base of the ice generates strong multiples which may mask for secondary phases. This effect may be crucial for acquisition of reflection seismic profiles on ice caps. Our experience shows that it is essential to use optimum depth for the charges and to seal the boreholes carefully.

Key Words: Active sources, seismology, Greenland, seismics on ice

1. Introduction

The recent global geo-community interest in the polar regions brings new challenges to the logistics and scientific setup of experiments in these unfriendly environments. The presence of ice caps and extreme weather conditions require reassessment of the approaches and techniques to be used for geophysical data acquisitions.

In this paper we share our experience of conducting a successful controlled source seismic experiment on top of the ice sheet in east-central Greenland from the viewpoint of technical issues of planning and conducting a controlled source seismic acquisition campaign, together with the challenges experienced in post-experiment data processing. Our analysis suggests that proper pre-planning of the experiment is crucial for the success of the experiment, in addition to the large logistic challenges of operating on the ice cap. We hope our observations are helpful to the future seismic experiments, and that they may assist in reducing a number of unpleasant surprises that may be met when working on the ice caps.

Although we do not address the crustal structure *per se*, we find it important to provide some geological/tectonic information on objectives of the project. The conjugate Atlantic passive margins of western Norway and eastern Greenland are characterized by the presence of coast-parallel mountain ranges with peak elevations of more than 3.5 km close to Scoresbysund in eastern Greenland and above 2000 m in Norway. These mountains are located far from the nearest plate boundary, which is the spreading ridge in the North Atlantic Ocean. There is substantial evidence that they have been uplifted during the latest 65 My *(Japsen and Chalmers,*

2000; Anell et al., 2009), although some authors believe that the topography already came into existence during the Caledonian Orogeny at around 440 Ma *(Nielsen et al., 2002)*. The issue of recent uplift in Norway is heavily discussed, because there is no sedimentary cover in onshore Norway, which prevents determination of a maximum age of the uplift. However, the offshore shelf and their sedimentary basins provide evidence for significant vertical displacement up to present time, including km-scale subsidence of the shelf and basins therein during the last 1-2 My *(Faleide et al., 2002; Faleide et al., 2008; Anell et al., 2010)*.

Understanding the causes of these pronounced and fast changes in topography requires knowledge of the crustal and mantle structure. A series of seismic experiments have recently been carried out, many as part of the TopoEurope programme *(Cloetingh et al., 2007; Cloetingh et al., 2009)*. In southern Norway and western Sweden the MAGNUS experiment operated about 60 seismometers for a period of 2 years *(Weidle et al., 2010; Maupin et al., 2013)*. A main result from this experiment is that the upper mantle velocities change abruptly from the topographically low Baltic Shield in Sweden into the high topography of Norway *(Medhus et al., 2012)*. This change is accompanied by a change from shield type crust to a crust lacking a high-velocity lower crust *(Stratford et al., 2009; Stratford and Thybo, 2011; Frassetto and Thybo, 2013; Loidl et al., 2014)*, which is similar to much of the crustal structure on the continental shelf *(Kvarven et al., 2014)*.

There is very little information available on the crustal structure in Greenland *(Artemieva et al., 2006; Artemieva and Thybo, 2008)* where the topographic change is better documented than in Scandinavia due to the presence of sedimentary and volcanic rocks at high altitude. The presence of Jurassic rocks *(Dam and Surlyk, 1998)* at almost 1000 m altitude in interior

Greenland shows that the topography cannot be caused by the Caledonian orogeny alone. Further, volcanic rocks of the North Atlantic Igneous province, related to the break-up of the North Atlantic at the beginning of the Tertiary *(Brooks, 2011)* are now found at altitudes up to 3700 m. Although there is uncertainty regarding the altitude at which the volcanic rocks solidified, this observation indicates that there has been substantial vertical movement during the Cenozoic. The seismic structure of Greenland is mainly known from active seismic experiments in the coastal regions with airgun sources *(Dahl-Jensen et al., 1998; Schmidt-Aursch and Jokat, 2005; Voss and Jokat, 2007; Voss et al., 2009)*. In interior Greenland, only five receiver function measurements of Moho depth have been published although with substantial uncertainty *(Kumar et al., 2007)* which may be due to the possible presence of a high-velocity lowermost crustal layer, that may be seen as either mantle or lowermost crust in the receiver functions *(Artemieva and Thybo, 2013)*.

A crustal seismic wide-angle refraction/reflection profile was acquired in the summer of 2011 on top of the Greenland ice sheet (Figure 1). This was the first active seismic experiment in inland Greenland. One of the challenges of the project is the presence of a thick 2-3.5 km ice sheet overlying the basement rock. In this paper we describe aspects of the techniques that were applied for acquiring the refraction seismic profile on top of the ice cap. We present recordings of the seismic waves in terms of record sections, and we analyse the source efficiency regarding energy output, frequency content and signal form.

2. Field technique

The TopoGreenland experiment was designed to provide information on the seismic structure of the crust and upper mantle in central Eastern Greenland. Ten broadband

seismometers were deployed for a period of 3 years on the ice cap and 13 seismometers were deployed on bed rock outside the ice cap for a period of 2 years. The data from this experiment is currently being analysed.

These first measurements of seismic structure in the interior of Greenland by the seismic refraction/wide angle reflection method were also carried out by the TopoGreenland experiment. Acquisition of geophysical data in onshore Greenland is logistically complicated by the presence of an up to 3.4 km thick ice sheet, permanently covering most of the land mass. Previous seismic surveys have only been carried out offshore and near the coast of Greenland, where the crustal structure is affected by oceanic break-up and may not be representative of the interior of the island. A controlled source seismic experiment was carried out in the summer of 2011 along an EW trending profile at the southern margin of the study area of the broadband experiment (Figure 1). Six scientists acquired the data during a period of two months. They were flown to the Summit camp in the center of Greenland by the US Coast Guard. From there they travelled independently on snow mobiles each dragging two sledges for carrying supplies, equipment, tents and personal supplies. Depots of fuel, explosives and other supplies had in advance been deployed from the air by parachuting. The team used about 12,000 l of fuel for driving and drilling as well as 5 tons of TNT for the sources of the experiment. The profile is 320 km long and the team drove about 22,000 km on the snow mobiles to complete the data acquisition. Severe weather conditions delayed the data acquisition twice by withholding activities for about two weeks in total.

The experiment involved drilling of 50 boreholes to ca. 80 m depth, loading each borehole with about 100 kg of TNT, and sealing the borehole with water in plastic bags. The drilling was carried out by use of hot water injected into the borehole under high pressure. The operation used about 1 ton of water per hour, equivalent to 3 m^3 of snow that had to be shoveled. The drilling operation lasted about 1½ month after when the 350 Texan instruments (Reftek-RT125) were deployed by three teams. Explosive charge sizes were 1 ton at the ends and ca. 500 kg along the profile, loaded with about 100 kg at 35-85 m depth in individual boreholes. The planned extension of the profile to the east coast of Greenland by use of OBSs and air gun shooting in Scoresbysund Fjord was unfortunately cancelled because access was prevented by ice drift. The shooting was done in about eight hours by two teams starting from the headquarters at the center of the profile. The collection of the instruments lasted about 1 full day, after when the data was uploaded to a central computer. The whole operation was very labor intensive, and we strongly acknowledge the efforts of the whole team.

The acquired data is of remarkably high quality for acquisition on an ice cap. Knowledge about explosive source efficiency in ice for seismic observation is very sparse. We used a different shooting strategy than employed by *(Kanao et al., 2011)* in Antarctica. In the following we present the data quality and analyse its characteristics regarding signal to noise ratio, frequency characteristics, and compare these characteristics to the quality of controlled source seismic data acquired on the continents exemplified by data from Kenya by the KRISP experiment *(Jacob et al., 1994)*.

3. Data analysis

The seismic records (Figure 2) show a strong refracted ice wave and refracted crustal phases (Pg) as well as clear mid-crustal and Moho (PmP) reflections. The amplitude of the refracted mantle phase (Pn) is weak and processing is required to identify it. The resulting seismic sections are of high quality for further interpretation and modelling. We analyse amplitudes and power spectra of the phases which are used for crustal modelling. We further analyse the background noise levels in detail.

For the amplitude study, the raw seismic sections (in SEG-Y format) are used. No filtering or any kind of gain control is applied prior to the amplitude information extraction. The amplitudes of the selected phases are extracted from the seismic sections based on the traveltimes picked for the interpretation of a crustal model. For each phase the traces are time-windowed around the picked time to assess the amplitude values. The time-window is defined from 100 ms before to 400 ms after the relevant picked time, resulting in a 500 ms time-window containing the phase of interest. For each trace, the maximum amplitude is extracted from the time-window. As a result, an amplitude vs offset dataset is determined for each phase of interest.

The noise level is estimated for each trace by similar method as for the processing of the amplitudes of the phases. A 100 s long time-window is selected 200 s after the first arrivals – based on the assumption that the predominant signal so long after the shot represents the background noise. For the selected time window, maximum and mean amplitudes of the background noise are determined.

Fourier spectra are calculated for the phases of interest and for the background noise. The spectra are computed only within the time-windows defined above. The resulting spectra plots

(Figure 3) show the frequency shifts with offset from the shot point. However, due to the short (500 ms) time window used in phase spectra computation, frequencies below 2 Hz cannot be analysed.

4. Results

The analysis of the amplitudes of different seismic phases shows distinct variability along the profile as exemplified by the largest shots at both ends of the transect, shot point 1 and 8 (Figure 3, top panels). A general observation is that the amplitude of the direct ice wave is the highest for all shot points within 120 km offset. The observed cyclic changes in the amplitude of the ice wave may be originating from constructive/destructive interference with the reflection from the base of the ice. It is characteristic that these amplitude undulations are largest in the eastern direction, i.e. in the direction where the ice thickness decreases, such that the effect is largest for shot point 8, although it is observed in all shots records. Direct comparison of the amplitudes is problematic for the ice wave from all sources (Figure 4) as the power of the sources varies by a factor of 2-5. The best fitting straight lines show similar slope for the power decrease with distance for all but number 4 the smallest shot for which the attenuation of the seismic waves appears to be slightly smaller than for the other sources. Otherwise the differences in amplitude among the recordings for the various shots seem to be primarily related to the difference in charge size.

The Pg phases are recorded out to 150-200 km offset in the eastern direction and to around 300 km offset in the western direction (Figure 3). This difference in recording offset is mainly caused by the difference in noise levels between the eastern and western ends of the profile. This

amplitude difference corresponds to a factor of 5-11 and suggests differences in attenuation of the seismic energy between the two ends of the profile. Similar observation is made from comparison of the Pg amplitudes from all shots records (Figure 5), where the general trend toward lower amplitudes for shots around the centre of Greenland is noticeable. This observation may be explained by differences in the coupling between the ice and the bedrock. It is possible, that the basal melting of the ice sheet is not uniform, and that a larger amount of melt is present in the deeper central section under the ice sheet than in the shallower part in the east. This could result in lower transmission from the ice to the basement for shot points in the centre of Greenland than closer to the coast. In this case the Pg waves will be stronger for the eastern than western shot points. The slopes of the best fitting straight lines are similar for most of the shot points, indicating that the attenuation within the crystalline crust of the Pg waves does not change along the profile, although we notice that the slopes are steeper for shot points SP3 and SP5, which indicates strong attenuation.

The amplitudes of Moho reflections are similar to the Pg level for all shot points at the relevant offsets beyond 80-100 km (Figure 6). The comparison of the reflection phases is more challenging than the refracted phases, because our modelling results reveal little lateral variability in the internal crustal velocity structure, whereas there are significant changes in Moho depth from 46 to 37 km. The Moho is deepest under central Greenland and shallows towards the coast. However, the observed amplitudes are everywhere above the noise level for the sources used in the experiment.

Mantle refractions are the weakest recorded phases. They are identified only for three shot points (Nos. 1, 2 and 8). The amplitude of this phase is close to the maximum noise level, which

makes the analysis uncertain. Furthermore, the arrival is identified only on a few traces, which prevents proper statistical analysis. The maximum amplitudes of the Pn are similar to the Pg at the same distance, but drop very rapidly with distance. Over the offset interval from 200 to 220 km the amplitude of the Pn phase drops by a factor of 10-11 to a level below the background noise.

We have also analysed the noise level at all receiver locations and compared the amplitudes of the ice and Pg waves for all sources. A time window from 200 to 300 s after the first arrival ensures that the effect of ice multiples is minimal. The overall noise level gradually increases towards the coast. The measured noise levels for the two end-shots (Figure 7) illustrate a clear eastward increase of the noise level. As oceanic waves and storms in the northern Atlantic Ocean are the major sources of the seismic noise in the region, the observed noise levels fit the expectations. The stations located more than 200 km away from the coast show a constant mean noise level ca 4-5 time lower than the stations close to the coast.

Frequency analysis of the data (Figure 3) shows that the energy of the ice wave is mainly concentrated in the range from 15 to 40 Hz with a bimodal distribution around 20 and 35 Hz and with little changes with offset. The frequency of the Pg and PmP phases ranges from 10 to 25 Hz in the near to mid distances and decreases to 5-15 Hz at large offsets. The Pn spectrum is questionable due to the small number of traces, but presumably concentrated around 8-10 Hz. The noise is mostly localized in the low frequency end between 1 and 8 Hz. Therefore simple band-pass filtering of the data leads to a significant improvement in signal/noise level at near offsets. However, frequency separation of the crustal phases from the ice wave is inefficient at small offsets (Figure 3).

Analysis of the data with respect to shot charge and detonation depth (Figure 8) indicates a linear relation between the peak amplitudes and charge load for the measured amplitudes of the ice and Pg phases at 20 and 60 km distances. The best fitting lines to our observations (Figure 8a) indicate an increase in amplitude of the seismic signals by a factor of 20-25 from the smallest to the largest charges. Our charge distribution from 200 to 1000 kg TNT corresponds to a factor of 5, which corresponds to a similar energy difference or an amplitude difference of 25, which is comparable to our observations. The dependence of the maximum identifiable offset with respect to the shot charges is less clear (Figure 8c), although a slight increase with charge is indicated. The charge distribution from 200 kg to 1000 kg corresponds to a change in the maximum offset of identifiable phases from 120 to 290 km.

The charge depth plays a major role for the recorded amplitudes (Figure 8b,d). Constructive interference between direct wave and surface multiple is expected when the source is located at depth below the surface corresponding to ¼ of the dominating wavelength. For the ice conditions in Greenland the optimal depth was estimated prior to the experiment to be around 60-65 m for a dominant frequency of 15 Hz and a velocity of 4000 m/s for the ice wave. The data obtained from the experiment (Figure 8) shows that the maximum amplitudes and offsets are obtained for the source located at 60-64 m depth. We have plotted the results in the charge – depth space for the maximum offset and the peak amplitude of the Pg wave at 20 km offset (Figure 8e,f). The best results are expected at similar depth, but the relevance of the borehole depth seems to decrease with the charge size.

We finally compare the data recorded on the Greenland ice cap with the shot records from a conventional onshore experiment (Figure 9), represented by the results of the KRISP90

experiment in Kenya *(Jacob et al., 1994)*. We compare the amplitudes for a land shot in Kenya with 840 kg of TNT with shot point 1 (1000 kg of TNT) of this study. The overall trend shows that the amplitudes of all phases for the ice shot are smaller than the conventional experiment with a slightly smaller charge size. The amplitude difference is about 1 order of magnitude and is almost constant with offset. The noise levels are comparable between the two experiments. The differences in the amplitudes may reflect: (1) differences in packing around the charges, (2) the presence of the thick ice sheet, resulting in seismic energy being trapped within the ice layer. The latter, is controlled by the seismic transmission characteristics from ice to basement, which may heavily depend on the presence of a water layer at the base of the ice cap. Most probably the ice layer traps a large portion of seismic energy as multiples in the ice, and there is indication that the eastward thinning of the ice cap leads to more efficient trapping in that direction (Figure 2 and 3).

5. Conclusions

This study demonstrates that controlled source seismic experiments on thick ice are possible and can be very successful. The general techniques used for conventional field acquisition are applicable to ice conditions. However, there are special issues to consider for planning seismic experiments on ice caps.

The presence of the ice generates strong multiples, which may trap substantial amounts of seismic energy. The energy penetration through the ice-basement may be limited, which leads to an order of magnitude decrease in amplitudes compared to conventional setup. Taking this into account, in order to maximize the recorded signal, proper identification of the optimal depth for

the shot point is essential. Our results indicate that a change in borehole depth by 10 m can cause a factor of 3 change in amplitudes.

Acknowledgment

We acknowledge the great effort of the other participants of the field team: Bob Greschke, Galen Kaip, Zurab Chemia, Asbjørn Bruun and Sönke Reiche. We thank the Danish Natural Research Council and Carlsberg Foundation for financial support. We thank the editor M. Kanao and two anonymous reviewers for their detailed comments.

References

Anell, I., Thybo, H., Artemieva, I.M., 2009. Cenozoic uplift and subsidence in the North Atlantic region: Geological evidence revisited. Tectonophysics 474, 78-105.

Anell, I., Thybo, H., Stratford, W., 2010. Relating Cenozoic North Sea sediments to topography in southern Norway: The interplay between tectonics and climate. Earth and Planetary Science Letters 300, 19-32, doi:10.1016/j.epsl.2010.1009.1009.

Artemieva, I., Thybo, H., 2008. Deep Norden: Highlights of the lithospheric structure of Northern Europe, Iceland, and Greenland. Episodes 31, 98-106.

Artemieva, I.M., Thybo, H., 2013. EUNAseis: A seismic model for Moho and crustal structure in Europe, Greenland, and the North Atlantic region. Tectonophysics, doi:10.1016/j.tecto.2013.1008.1004.

Artemieva, I.M., Thybo, H., Kaban, M.K., 2006. Deep Europe today: Geophysical synthesis of the upper mantle structure and lithospheric processes over 3.5 Ga, in: Gee, D.a.S., R. (Ed.), European Lithosphere Dynamics, Geological Society London Sp. Publ., London, pp. 11-41.

Brooks, C.K., 2011. The East Greenland rifted volcanic margin. Geol. Surv. Denmark Greenland Bull. 24, 96 pp.

Cloetingh, S., Thybo, H., Faccenna, C., 2009. TOPO-EUROPE: The Geoscience of coupled Deep Earth-surface processes Peter Ziegler Dedication. Tectonophysics 474, 1-2.

Cloetingh, S., et al., 2007. TOPO-EUROPE: The geoscience of coupled deep Earth-surface processes. Global And Planetary Change 58, 1-118.

Dahl-Jensen, T., Thybo, H., Hopper, J., Rosing, M., 1998. Crustal structure at the SE Greenland margin from wide-angle and normal incidence seismic data. Tectonophysics 288, 191-198.

Dam, G., Surlyk, F., 1998. Stratigraphy of the Neill Klinter Group; a Lower - lower Middle Jurassic tidal embayment succession, Jameson Land, East Greenland. Geology of Greenland Survey Bulletin 175, 1-80.

Faleide, J.-I., et al., 2002. Tectonic impact on sedimentary processes during Cenozoic evolution of the northern North Sea and surrounding areas. Geological Society Special Publications 196, 235-269.

Faleide, J.I., Tsikalas, F., Breivik, A.J., Mjelde, R., Ritzmann, O., Engen, O., Wilson, J., Eldholm, O., 2008. Structure and evolution of the continental margin off Norway and Barents Sea. Episodes 31, 82-91.

Frassetto, A., Thybo, H., 2013. Receiver function analysis of the crust and upper mantle in Fennoscandia – isostatic implications. Earth and Planetary Science Letters 381, 234-246.

Jacob, A.W.B., Vees, R., Braile, L.W., Criley, E., 1994. Optimization of wide-angle seismic signal-to-noise ratios and P-wave transmission in Kenya. Tectonophysics 236, 61-79.

Japsen, P., Chalmers, J.A., 2000. Neogene uplift and tectonics around the North Atlantic: overview. Global And Planetary Change 24, 165-173.

Kanao, M., Fujiwara, A., Miyamachi, H., Toda, S., Ito, K., Tomura, M., Ikawa, T., Grp, S.G., 2011. Reflection imaging of the crust and the lithospheric mantle in the Lützow-Holm complex, Eastern Dronning Maud Land, Antarctica, derived from the SEAL transects. Tectonophysics 508, 73-84.

Kumar, P., Kind, R., Priestley, K., Dahl-Jensen, T., 2007. Crustal structure of Iceland and Greenland from receiver function studies. Journal of Geophysical Research-Solid Earth 112.

Kvarven, T., Ebbing, J., Mjelde, R., Faleide, J.I., Libak, A., Thybo, H., Flueh, E.R., Murai, Y., 2014. Crustal structure across the Møre margin, mid-Norway, from wide-angle seismic and gravity data. Tectonophysics 626, 21-40.

Loidl, B., Behm, M., Thybo, H., Stratford, W., 2014. Three-dimensional seismic model of crustal structure in Southern Norway. Geophysical Journal International 196, 1643-1656.

Maupin, V. et al., 2013. The deep structure of the Scandes and its relation to tectonic history and present-day topography. Tectonophysics 602, 15-37.

Medhus, et al., 2012. Upper-mantle structure beneath the Southern Scandes Mountains and the Northern Tornquist Zone revealed by P-wave traveltime tomography. Geophys. J. Int. 189, 1315-1334.

Nielsen, S.B., et al., White, N. (Eds.), 2002. Exhumation of the North Atlantic Margin: Timing, Mechanisms and Implications for Petroleum Generation. Geological Society, London, Special Publications, London, pp. 45-65.

Schmidt-Aursch, M.C., Jokat, W., 2005. The crustal structure of central East Greenland - I: From the Caledonian orogen to the Tertiary igneous province. Geophysical Journal International, 160, 736-752.

Stratford, W., Thybo, H., 2011. Seismic structure and composition of the crust beneath the southern Scandes, Norway. Tectonophysics 502, 364-382.

Stratford, W., Thybo, H., Faleide, J.I., Olesen, O., Tryggvason, A., 2009. New Moho Map for onshore southern Norway. Geophysical Journal International 178, 1755-1765.

Voss, M., Jokat, W., 2007. Continent-ocean transition and voluminous magmatic underplating derived from P-wave velocity modelling of the East Greenland continental margin. Geophysical Journal International 170, 580-604.

Voss, M., Schmidt-Aursch, M.C., Jokat, W., 2009. Variations in magmatic processes along the East Greenland volcanic margin. Geophysical Journal International 177, 755-782.

Weidle, C. et al., 2010. MAGNUS-A Seismological Broadband Experiment to Resolve Crustal and Upper Mantle Structure beneath the Southern Scandes Mountains in Norway. Seismological Research Letters 81, 76-84.

Figure captions

Figure 1. Topographic map of Greenland and the bathymetry of the surrounding ocean. The dashed box shows the extent of the zoomed plot of the working area. The solid line shows the location of the refraction profile TopoGreenland-2011. The red circles mark the locations of the eight shot points along the profile. Small yellow circles mark the locations of the long-term deployed broad-band seismic stations. Numbering of the shots is from East to West (shown on the insert map).

Figure 2. Seismic sections of the two end-shot points recorded along the profile. The data was subject to gain control (de-bias, divergence correction, band-pass filter 0.5-50 Hz) to enhance late arriving reflections from the Moho. Similar overall good quality of the data is recorded for the entire profile.

Figure 3. Comparison of the amplitudes and power spectrums of the data acquired for the two end-shots. Left column: the westernmost shot point 8 (1000 kg of TNT); right column: the easternmost shot point 1 (1000 kg of TNT). The top panel shows the amplitudes of selected phases and the noise level as a function of distance from the shot point. For each phase a narrow time window around the picked arrival was analysed for the maximum amplitude (-0.1/+0.4 s). Color code for amplitude measurements: Gray – ice wave; green – Pg phase; blue – PmP reflections; and red – Pn refraction phase. For the noise analysis a time window of 100 s length starting 200 s after the first arrival was used to compute the mean and the maximum amplitude. The mean and max noise levels are shown as shades of gray. Following panels are power

spectrum plots computed for the phases stated above as marked on the left side. The spectrums are in absolute values for each sub-panel.

Figure 4. Plot of the amplitude of the Ice wave as a function of offset from the shot point in log-log space. The colors correspond to the individual shot points marked in the legend. Lines are the best fit for each shot point (black line is for shot point 1). Gray zone shows the average noise level.

Figure 5. Plot of the amplitude of the Pg wave as a function of distance from the shot point in log-log space. The colors correspond to the individual shot points marked in the legend. Lines are the best fit for each shot point (black line is for shot point 1). Gray zone shows the average noise level

Figure 6. Plot of the amplitude of the PmP wave as a function of distance from the shot point in log-log space. The colors correspond to the individual shot points marked in the legend. Lines are the best fit for each shot point (black line is for shot point 1). Gray zone shows the average noise level.

Figure 7. Comparison of the amplitudes of Ice and Pg phases with the maximum and mean noise levels for two shot records. Blue line – amplitude of the Ice wave; red line – amplitude of the Pg; pink shading – maximum noise level; violet shading - mean noise level. Red diamonds mark the location of the shot points.

Figure 8. Statistics of the efficiency (in terms of maximum amplitude and maximum detectable offsets for the seismic phases used in crustal structure modeling) for all 8 shot points as a function of charge size and borehole depth. Top panels (a, b) show the peak amplitude for Ice

and Pg waves recorded at 20 and 60 km offsets. Middle panels (c, d) show the maximum recorded offsets from the shot point. Bottom panels (e, f): maximum offset and peak amplitude of the Pg phase at 20 km offset, plotted in the charge size – borehole depth space. Black diamonds – actual shot data.

Figure 9. Comparison of the shot efficiency for ice and conventional environments (onshore shooting in the Kenya Rift). The amplitude data is taken for shot point 1: blue – ice wave; green – Pg; red – PmP; gray shading – mean noise level. The shaded areas are results for the KRISP90 experiment in Kenya, modified after Jacob et al. (*1994*): light blue - Pg amplitudes; pink – PmP amplitudes.

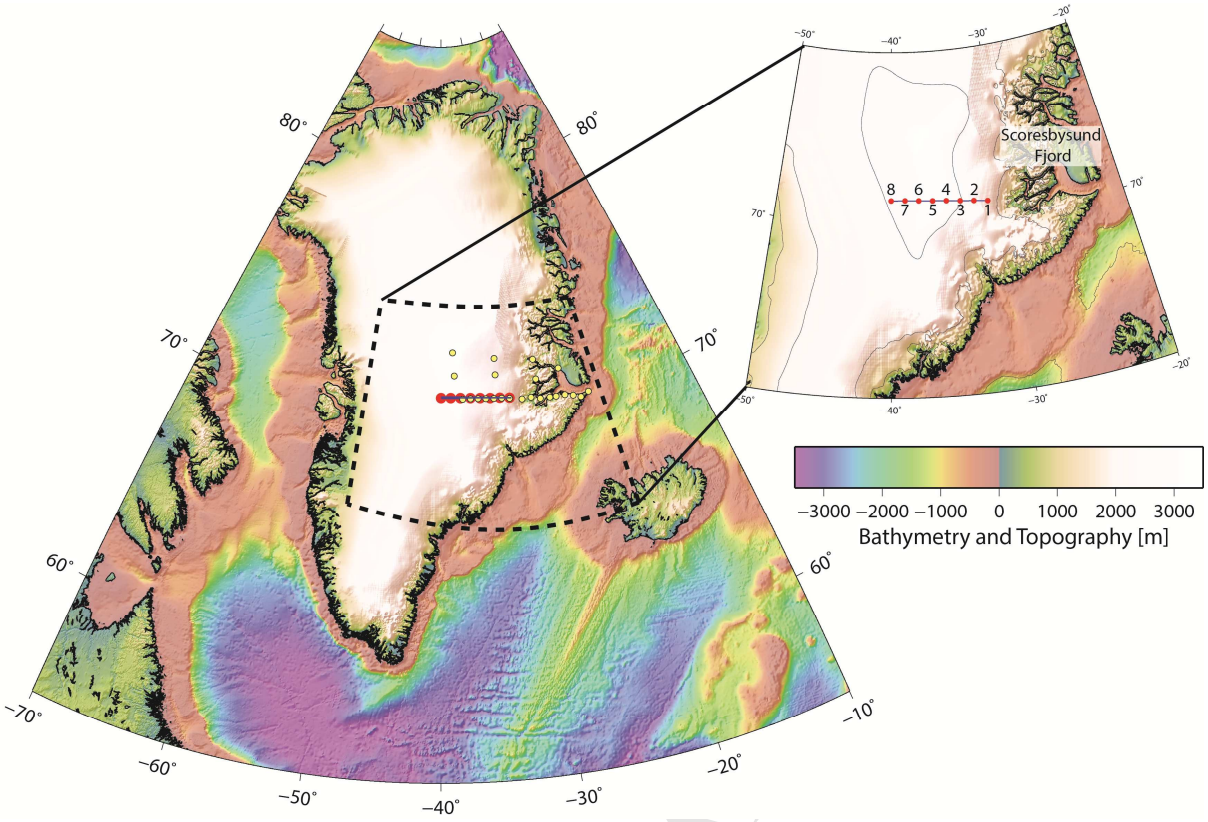
Scoresbysund
Fjord
8 6 4 2
7 5 3 1
−3000 −2000 −1000 0 1000 2000 3000
Bathymetry and Topography [m]

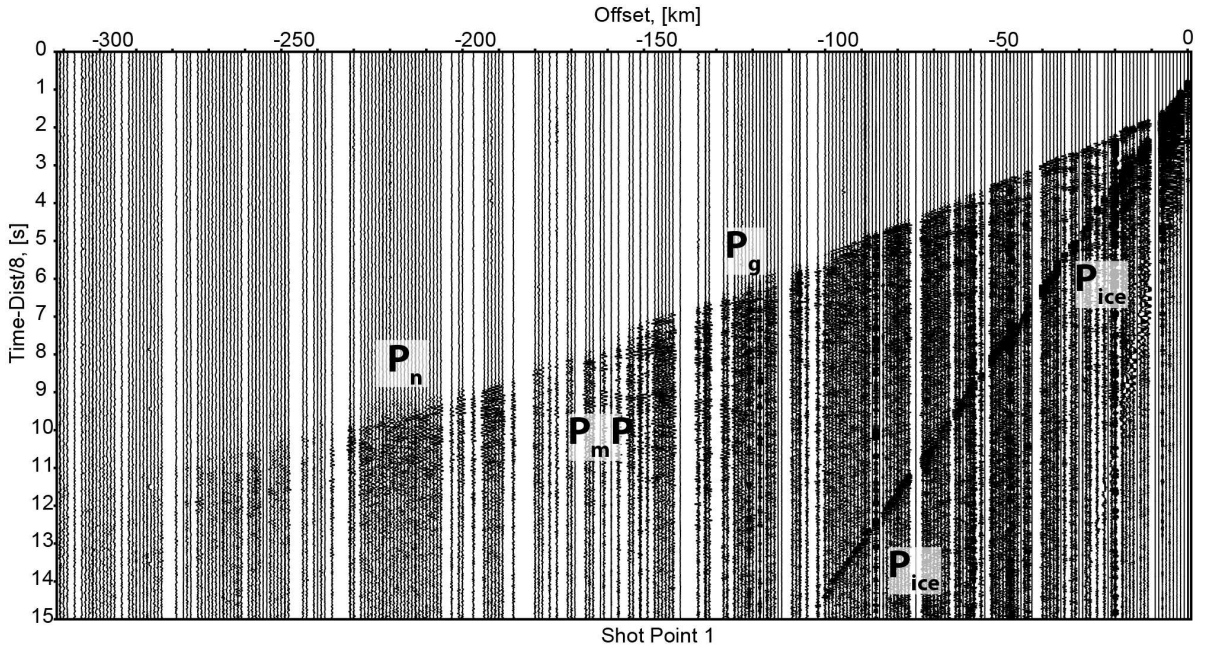
Offset, [km]
-300
-250
-200
-150
-100
-50
0
Time-Dist/8, [s]
0
1
2
3
4
5
6
7
8
9
10
11
12
13
14
15
P n
P m P
P g
P ice
P ice
Shot Point 1

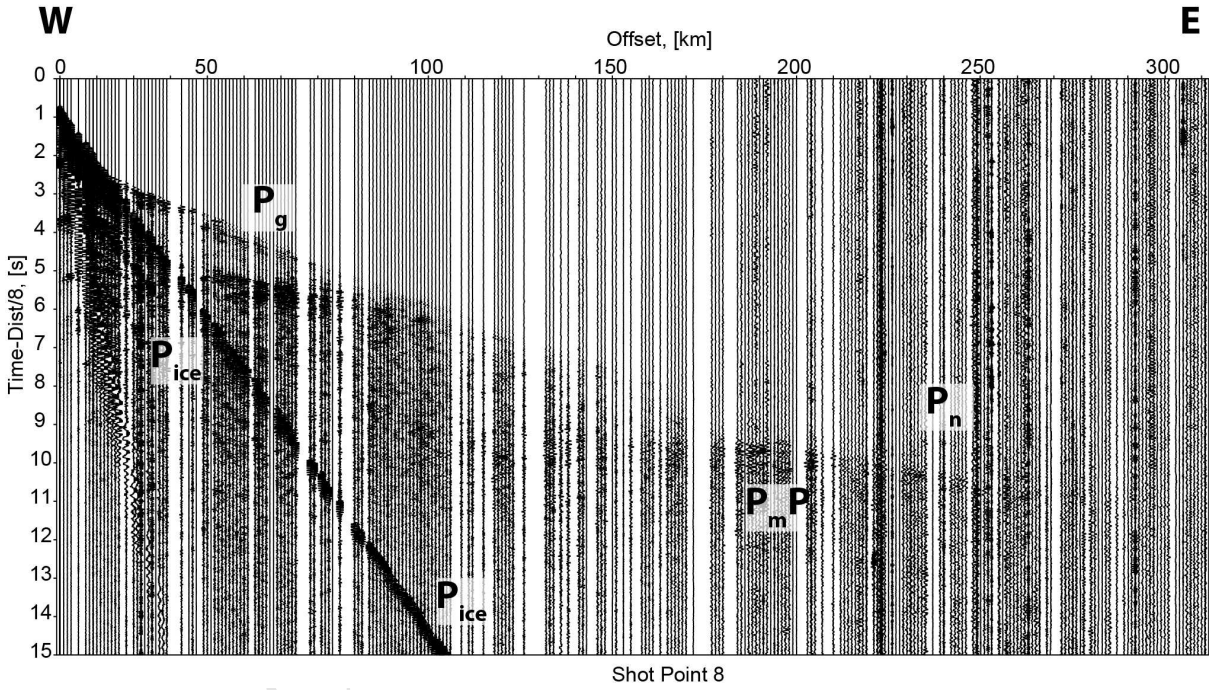
W
E
Offset, [km]
0
50
100
150
200
250
300
Time-Dist/8, [s]
0
1
2
3
4
5
6
7
8
9
10
11
12
13
14
15
P g
P ice
P ice
P n
P m P
Shot Point 8

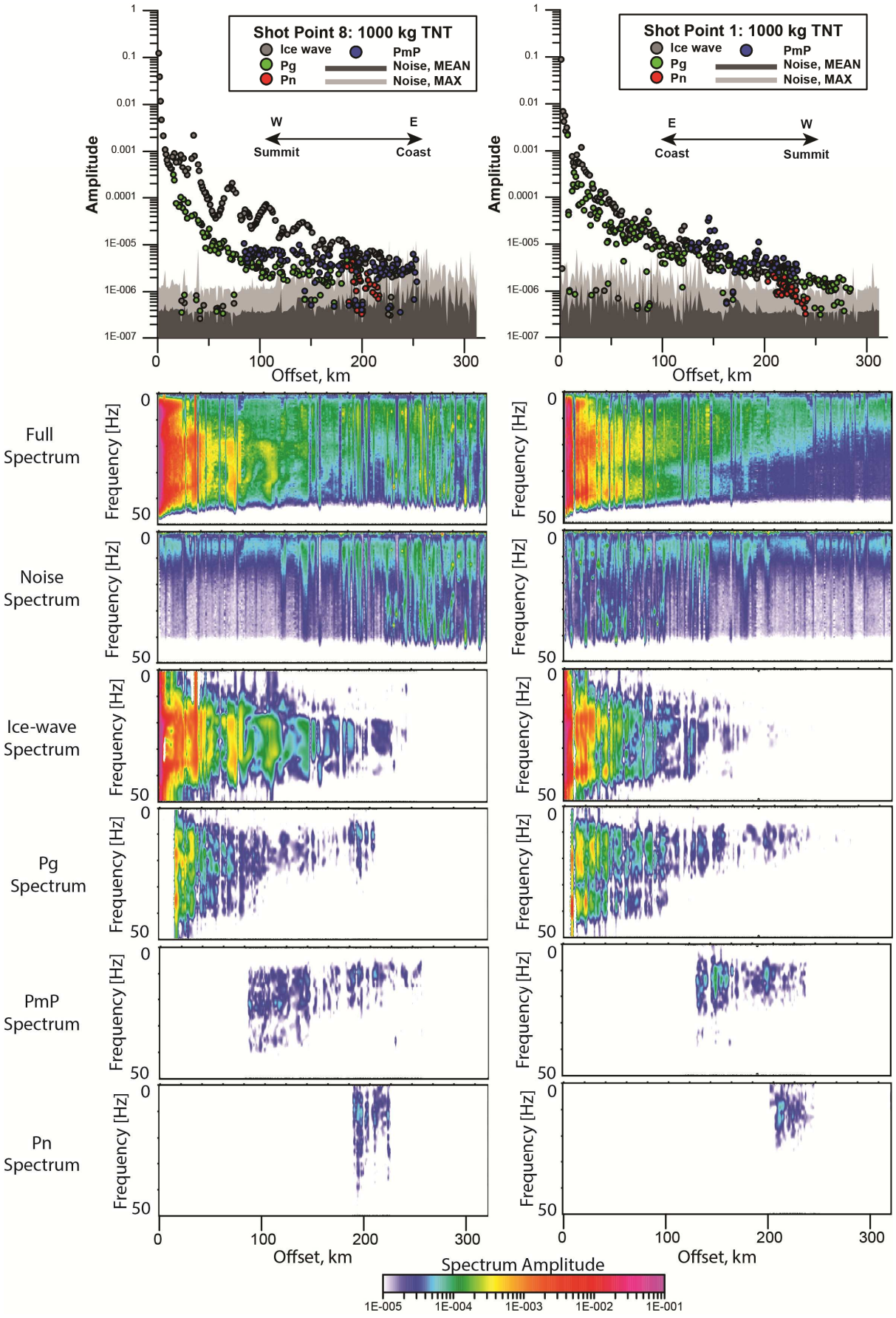
Shot Point 8: 1000 kg TNT
Ice wave
Pg
Pn
PmP
Noise, MEAN
Noise, MAX
W
Summit
E
Coast
Amplitude
Offset, km
Shot Point 1: 1000 kg TNT
Ice wave
Pg
Pn
PmP
Noise, MEAN
Noise, MAX
E
Coast
W
Summit
Amplitude
Offset, km
Full Spectrum
Noise Spectrum
Ice-wave Spectrum
Pg Spectrum
PmP Spectrum
Pn Spectrum
Frequency [Hz]
Offset, km
Spectrum Amplitude
1E-005
1E-004
1E-003
1E-002
1E-001

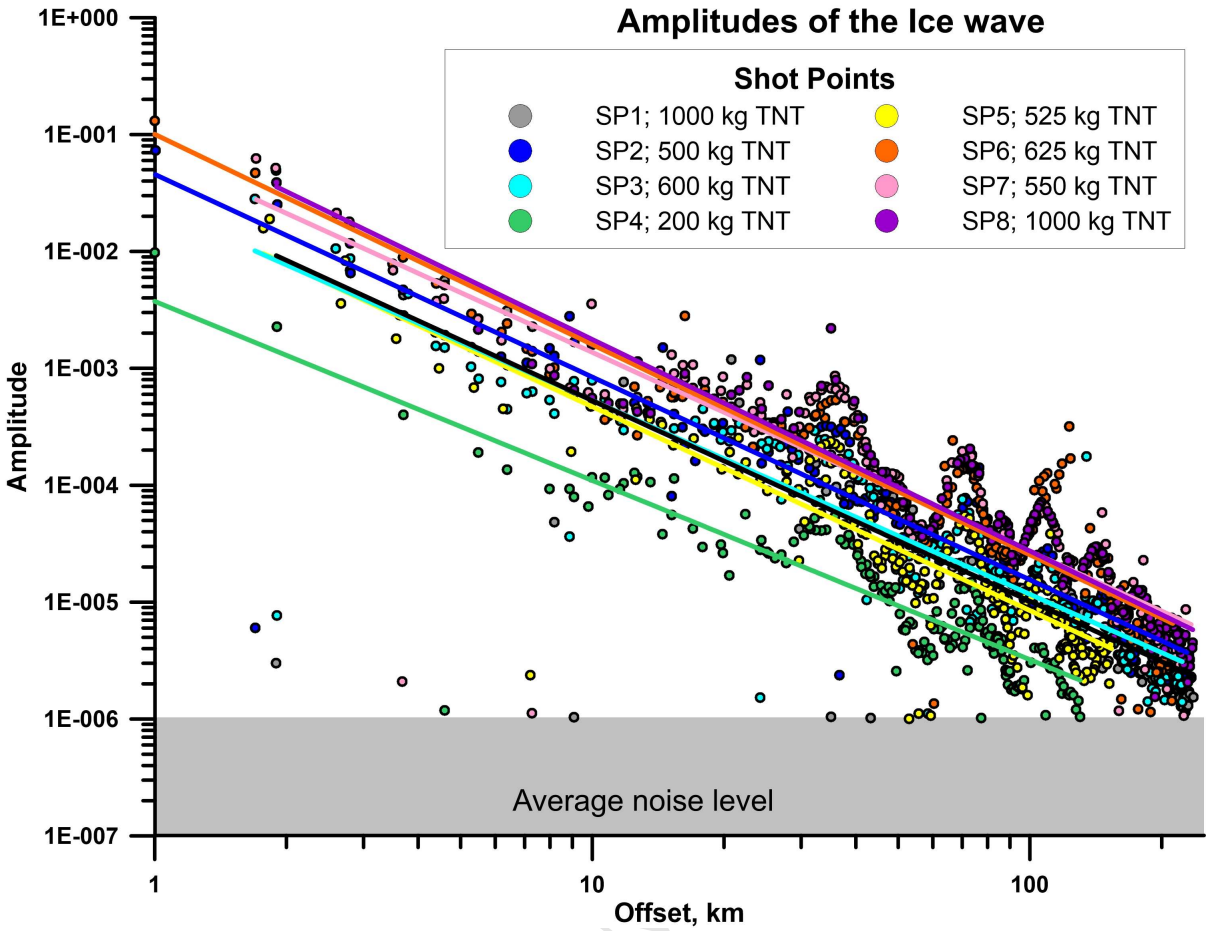

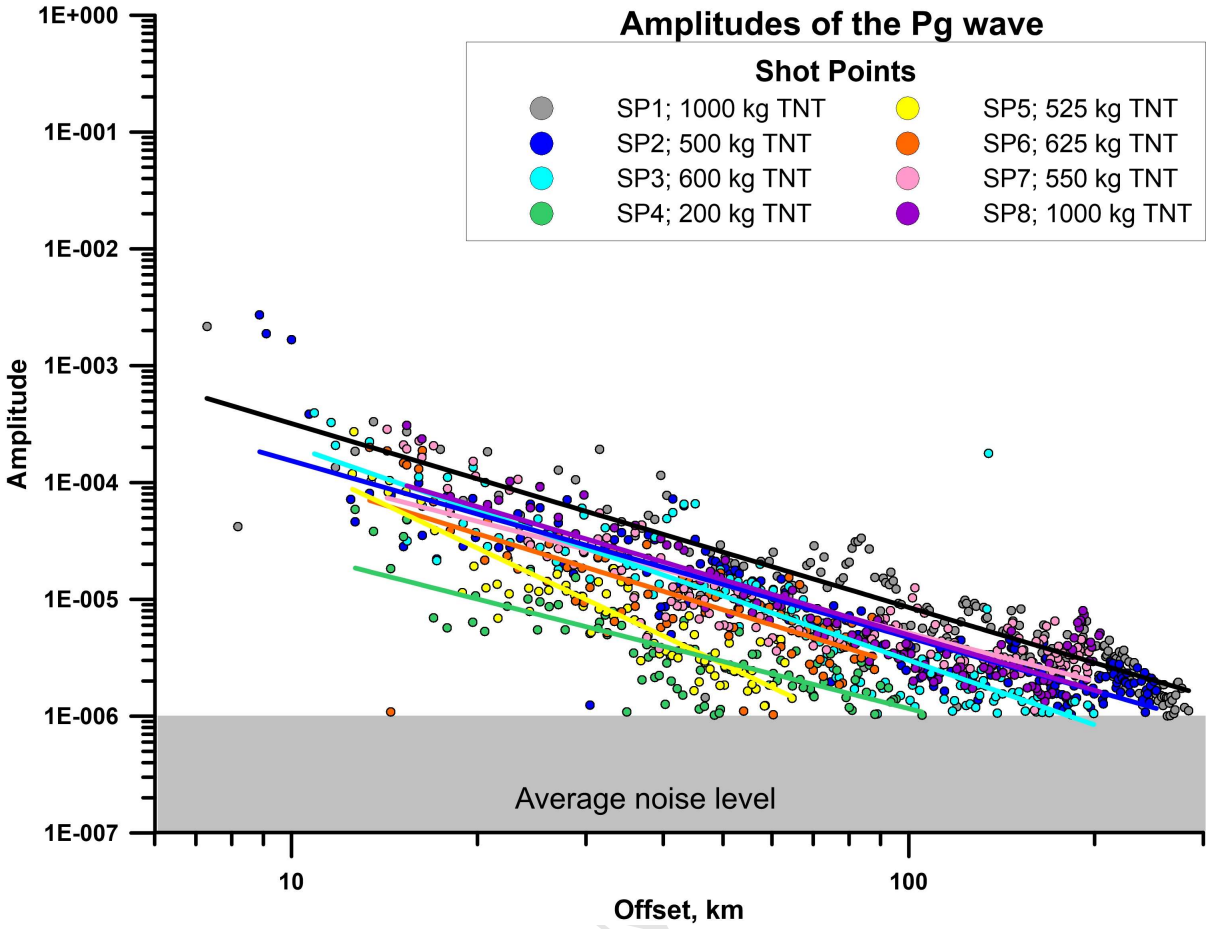

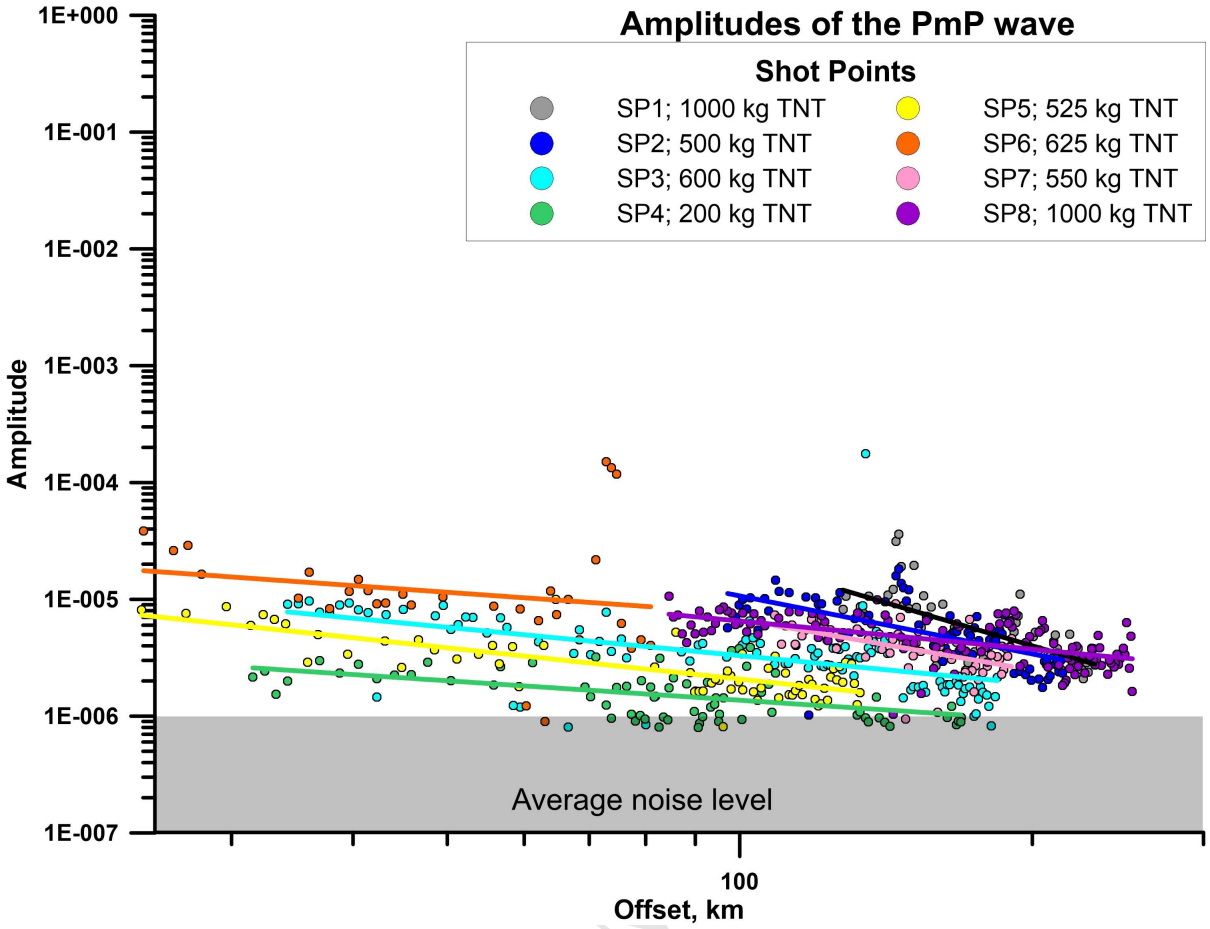

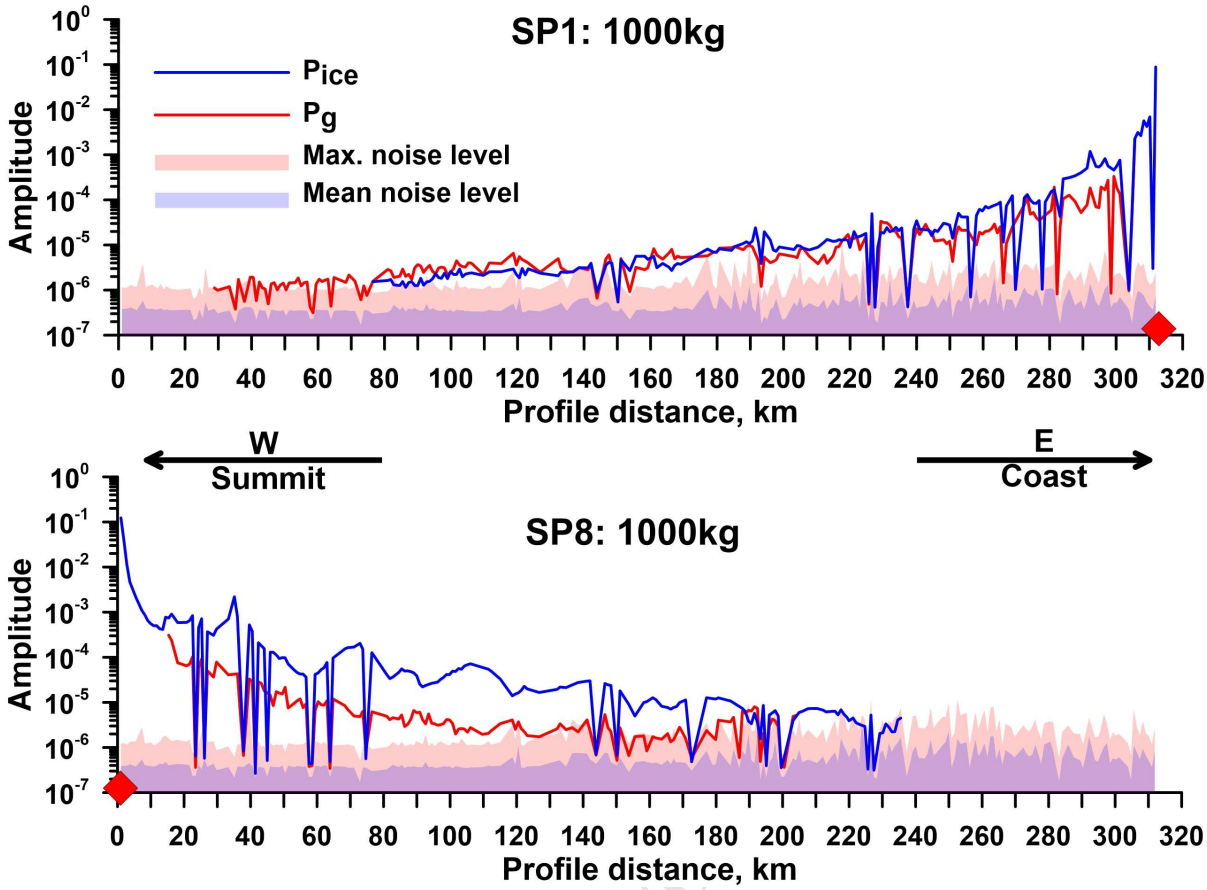

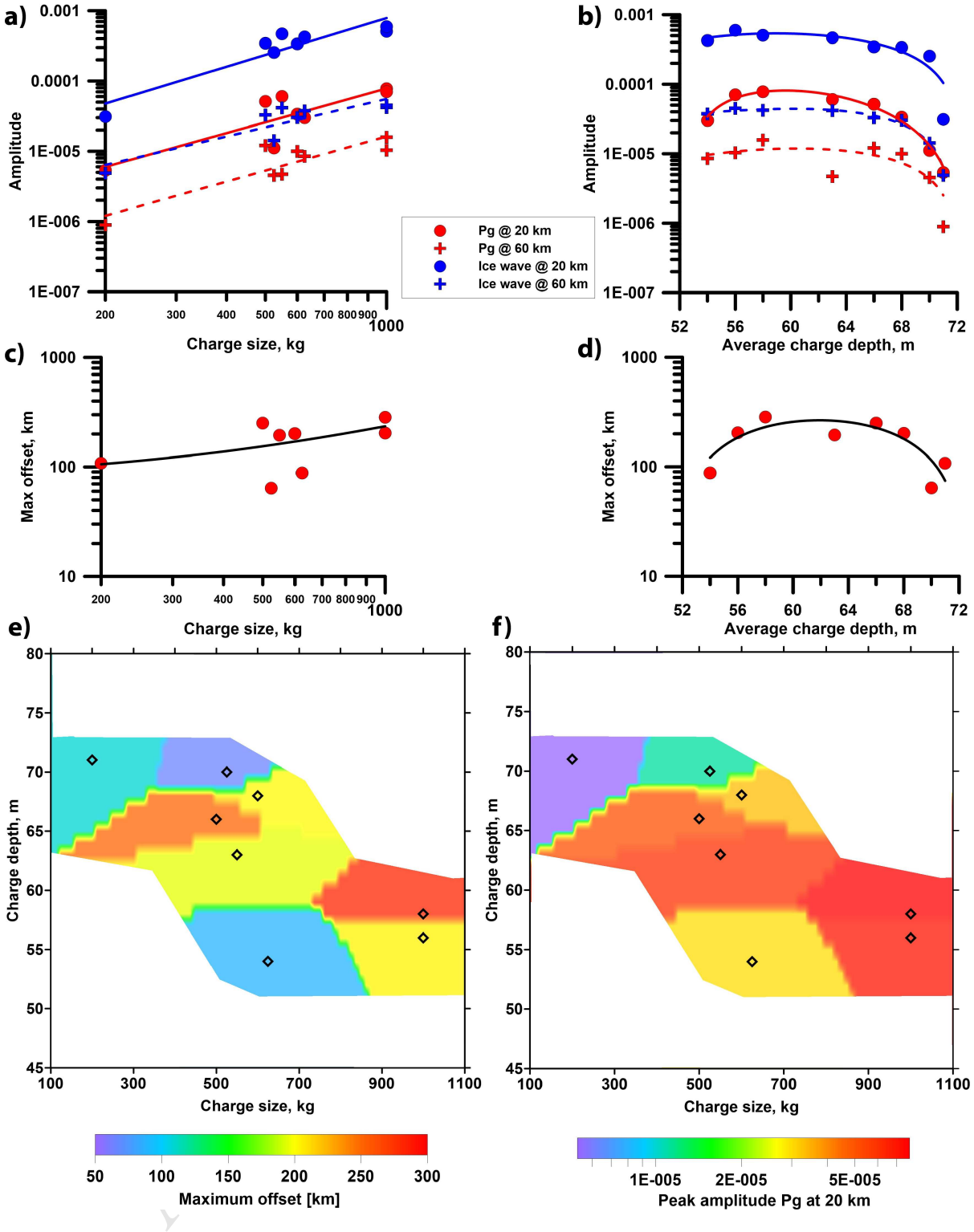
a)
b)
c)
d)
e)
f)
Amplitude
Charge size, kg
Average charge depth, m
Max offset, km
Charge depth, m
Pg @ 20 km
Pg @ 60 km
Ice wave @ 20 km
Ice wave @ 60 km
Maximum offset [km]
Peak amplitude Pg at 20 km